Journal of Applied Geophysics 153 (2018) 127–135

Contents lists available at ScienceDirect

Journal of Applied Geophysics

journal homepage: www.elsevier.com/locate/jappgeo

Probing the frontal deformation zone of the Chihshang Fault with boreholes and high-resolution electrical resistivity imaging methods: A case study at the Dapo site in eastern Taiwan

Chang Ping-Yu [a,e,*], Huang Wen-Jeng [b], Chen Chien-Chih [a], Hsu Han-lun [a], Yen I-Chin [b], Ho Gong-Ruei [a], Lee Jian-Cheng [c], Lu Shih-Ting [d], Chen Po-Tsun [d]

[a] Department of Earth Sciences, National Central University, Zhongli, Taoyuan, Taiwan
[b] Institute of Applied Geology, National Central University, Zhongli, Taoyuan, Taiwan
[c] Institute of Earth Sciences, Academia Sinica, Nangang, Taipei, Taiwan
[d] Central Geological Survey, MOEA, R.O.C., Taiwan
[e] Earthquake-Disaster & Risk Evaluation and Management Center, National Central University, Taiwan

ARTICLE INFO

Article history:
Received 5 October 2017
Received in revised form 6 March 2018
Accepted 8 April 2018
Available online 12 April 2018

ABSTRACT

Not only direct fault ruptures but also later mass movement may result in complicated frontal deformation of the faults. Consequently, the deformation front or the contacts between the unconsolidated materials from the hanging wall and footwall of the thrust fault may indicate the toe of the mass movement instead of the actual fault zone. In this study, we used a combination of surface electrical resistivity imaging methods and borehole records in order to investigate the geometries of the structures in the frontal deformation zone of the Chihshang Fault at the Dapo elementary school. From the cores, we observed three different geological components at the Dapo site: the conductive Lichi mélange of the hanging wall, the colluvial gravels and the underlying fluvial-gravel layer at the footwall. The resistivity images from two parallel survey lines reveal that the position where the fault trace was thought to be is actually the toe of the slumping body's surface ruptures consisting of materials from the Lichi mélange. On the basis of the resistivity images, we also found that the actual fault plane is located on the southeastern side of the resistivity survey line near the hilltop. As a result, we conclude that mass movement induced by the inter-seismic creeping, not direct faulting, is the main factor affecting the frontal deformation zone of the Chihshang fault at the Dapo site.

1. Introduction

It has been reported that direct fault ruptures as well as later mass movement may result in complicated frontal deformation of the faults (e.g., Lee et al., 2004). If a frontal deformation zone comprises a mixture of disturbed unconsolidated materials from both the hanging wall and the footwall, the actual fault zone will be difficult to differentiate from the mass-movement structures. In the current study, our efforts focus on the frontal deformation structures of the Chihshang Fault in the Dapo area of Taitung County, which is located in eastern Taiwan's longitudinal valley. It was regarded as a part of the Longitudinal Fault that divided the Eurasia continental plate from the Philippine Sea Plate. Previous studies showed that the Chihshang Fault is an active fault with distinctive fault scarps and aseismic creeping (e.g., Angelier et al., 2000; Lee et al., 2003; Shea et al., 2014). In addition, two earthquakes with the same magnitude of 6.8 took place on the Chihshang Fault in 1951 and 2008, respectively. The creeping fault like the Chihshang Fault that have generated earthquakes up to magnitude 6.8 in shallow continental regions could produce similar fault-surface rupture areas and similar peak ground shaking as their locked fault counterparts of the same earthquake magnitude (e.g., Harris, 2017). Hence it is important to investigate their creeping behaviors and deformation in the past few thousand years in order to access the earthquake hazard risks. The width of the frontal deformation zone of the Chihshang Fault ranges from tens to hundreds of meters. Lee et al. (2001) installed five creepmeters at the Dapo and Chinyuan sites and found a large horizontal shortening rate of 19.4 ± 0.3 mm/year and 17.3 ± 0.7 mm/year, respectively. However, the 4-year records of creepmeters show that the fault moved steadily during the rainy season but remained quiet during the dry season (Lee et al., 2003). The fact implies that not only fault creeping but also mass movement may play an important role in triggering the extraordinary shortening rate of the Chihshang Fault.

Researchers have often used the direct trenching or borehole methods (e.g., Carpenter et al., 2011; Chen et al., 2007; Lin et al.,

* Corresponding author at: Department of Earth Sciences, National Central University, Zhongli, Taoyuan, Taiwan.
E-mail address: pingyuc@ncu.edu.tw. (P.-Y. Chang).

https://doi.org/10.1016/j.jappgeo.2018.04.006
0926-9851/

2007) to investigate the fault geometries in the deformation zone of faults. However, borehole records have limited spatial information if the locations of boreholes are sparse; moreover, trenching approaches are expensive and excavations are usually limited to a depth of a few meters. These limitations of the "direct" observation methods make it difficult, without ample budgets, to delineate zones of frontal deformation in detail. Non-destructive geophysical methods, such as ground penetrating radar (GPR) (e.g., Cai et al., 1996; Chow et al., 2001; McClymont et al., 2008) and surface resistivity imaging methods (e.g., Colella et al., 2004; Nguyen et al., 2007; Suski et al., 2010), provide an alternative way to examine subsurface structures in an acceptable resolution. When these methods are combined with limited boreholes or trenching observations, one would be able to reconstruct detailed fault-zone geometries effectively. Suzuki et al. (2000) used electric and electromagnetic methods including a controlled-source magnetotelluric method and direct current resistivity imaging methods, in combination with trenching verifications, to explore geological structures covered by thick Quaternary formations at four active fault sites in Japan. Similarly, Chuang et al. (2014) carried out electrical resistivity imaging to recognize the geometrical characterization of active faults and to improve the tectonic knowledge of Greece's Tyrnavos Basin. In our current study at the Dapo site, we used the resistivity imaging method to identify the spatial relationships between the boreholes, since most of the geological materials are conductive in the area and the method can provide high-resolution subsurface profiles with depths of up to tens of meters.

2. Geological settings

The Chihshang Fault is located in the middle of the longitudinal valley and is believed to be part of the Longitudinal Valley Fault (LVF) of eastern Taiwan (Hsu, 1962). The NNE-trending LVF marks the active suture fault belts between the Costal Range at the Philippine Sea Plate and the Central Range at the Eurasia Plate (Fig. 1). The Central Range consists of mainly metamorphic rocks, whereas the Costal Range consists of the geological sequences of colliding volcanic arcs, such as the Lichi mélange, the sedimentary Fangshuliao formation, and the Duluanshan Andesites. The Chihshang Fault is a N18°E-trending reverse fault with thrust and left-lateral slipping components of movement (Angelier et al., 1997; Angelier et al., 2000). Studies from Surface outcrops and earthquake foci suggest that the fault plane of the Chihshang Fault is dipping at an angle of between 45° and 55° to the east (Angelier et al., 2000; Tsai et al., 1977). The Chihshang Fault is the tectonic contact between the Pliocene Lichi mélange to the east and the Pleistocene-Holocene fluvial deposits to the west in the Chihshang area. The Lichi mélange consists of various exotic rocks, such as volcanic, ophiolitic, and sedimentary rocks, in the matrix of mudstone and marine clays. And the fluvial deposits consist mainly of unconsolidated gravels and sands from either the Central Range or the Costal Range. Chow et al. (2001) conducted seismic reflection and GPR surveys in the Village of Chinyuan, southeast of Chihshang Township, along the topographic traces of the Chihshang Fault. They concluded that the fault zone consists of two parallel faults, which change their dipping and strike directions rapidly near the surface. Chow et al. (2001) also identified paleoseismic fault events by using geophysical-attribute indicators such as the upward termination of faults, the colluvial wedges on the downthrown side, and the sedimentary injection sills. Unfortunately, regarding the Chihshang Fault region, Chow et al. (2001) offers no direct comparisons between trenching profiles/boreholes and such geophysical exploratory profiles as GPR and seismic reflections. To further probe the deformation zone of the fault, it is hence necessary to carry out high-resolution geophysical surveys as well as borehole explorations along the same profiles.

3. Survey configurations

In the Dapo site, we completed seven boreholes and deployed two surface ERI survey lines for high-resolution imaging of the subsurface structures in the fault zone. Our research area was located next to the rod-type creepmeters, CHIH001 and CHIH002, installed for the previous research conducted by Lee et al. (2001). Fig. 2a and b shows the locations of surface ERI arrays, the creepmeters, and the borehole positions.

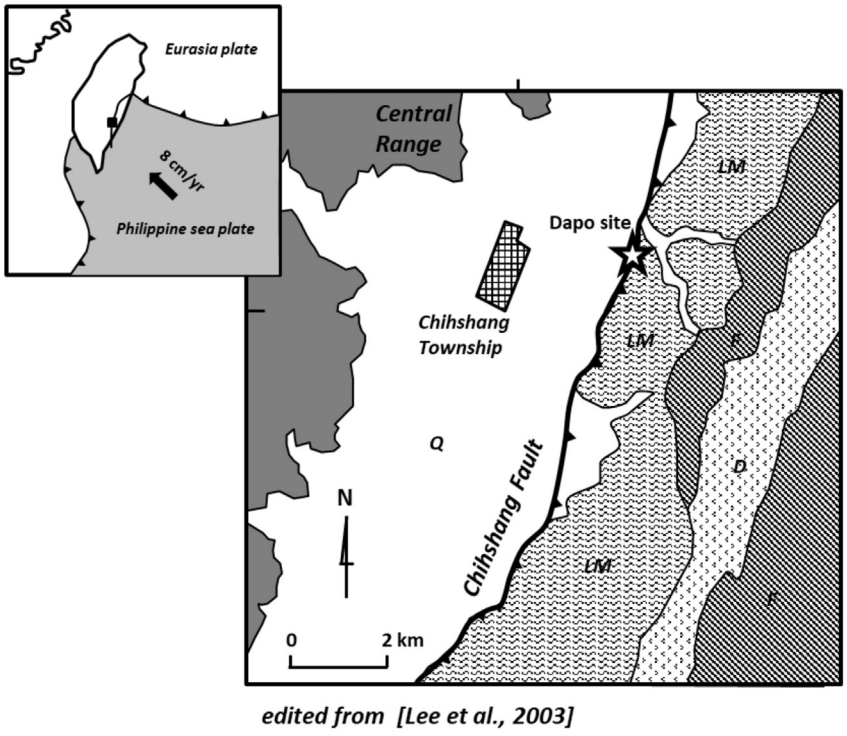

Fig. 1. The geology settings of the region near the Dapo site. Geological units D, F, LM, and Q represent the Tuluanshan Andesites, the Fangshuliao formation, the Lichi mélange, and the Quaternary deposits.

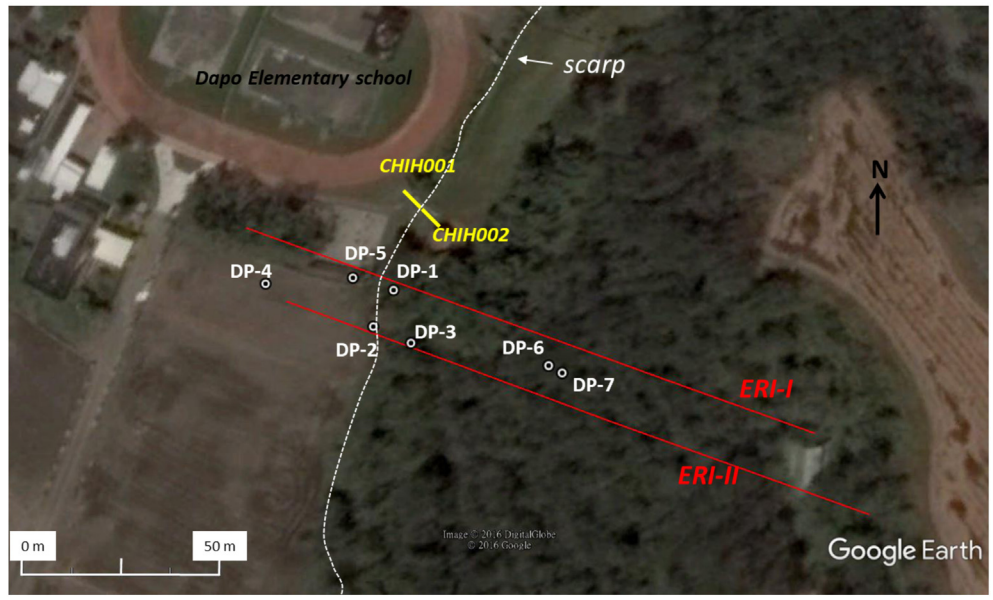

a

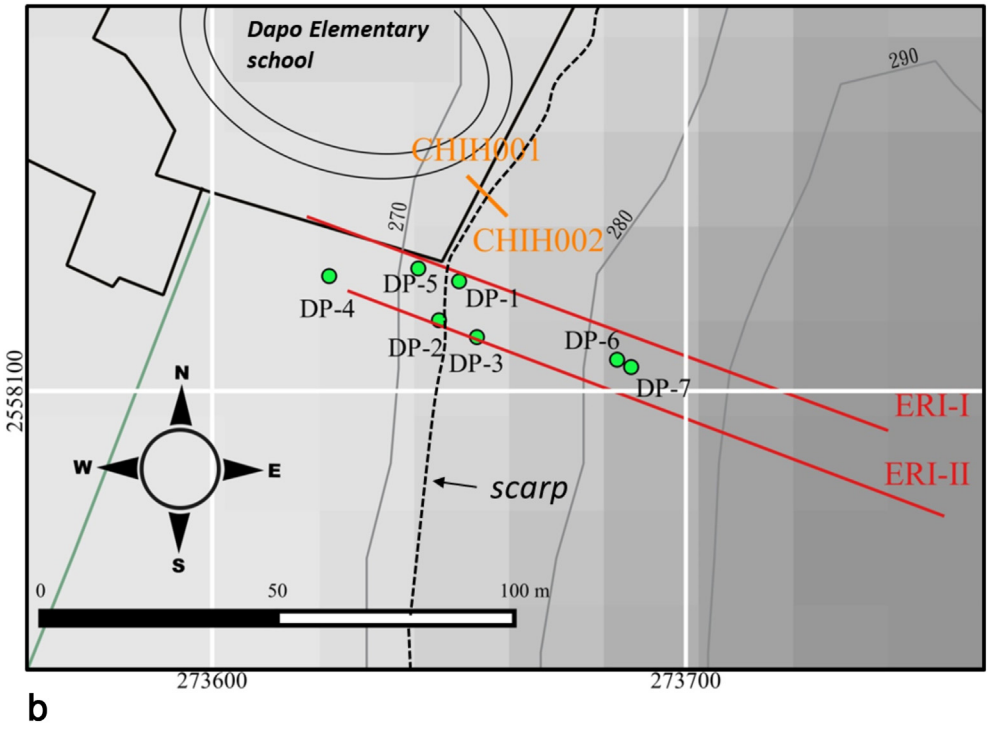

b

Fig. 2. (a): The satellite image of the Dapo site. (b): The topographic map and the configurations of the ERI survey lines, ERI-I and ERI-II, and the boreholes, DP-1 to DP-7, at the Dapo research site near the Dapo elementary school. CHIH001 and CHIH002 are the creepmeters installed for monitoring the activity of the Chihshang Fault.

We conducted the two ERI surveys, ERI-I and ERI-II, separately with 2-m electrode spacing along directions that are perpendicular to the surface rupture traces. The two parallel surface arrays are about 10 m apart. We deployed 64 electrodes in each array by interleaving the positions of the current (C) and the potential (P) electrodes. The surface ERI measurements were collected with a multi-channel system in arrays with all possible combinations of the interleaving current and potential electrodes. The system has 64 independent channels and measures the potential with 32 P electrodes concurrently while switching the two current channels from the other 32 C electrodes. Core samples were collected in four boreholes, DP-1, DP-4, DP-6, and DP-7 so that we could correlate the resistivity profiles to the core records. In addition, we also used boreholes DP-1, DP-2, DP-3, DP-4, DP-5, and DP-6 for installing the borehole electrodes for a long-term monitoring study of electrical resistivity. The depths of boreholes DP-1, DP-4, and DP-6 reached about 30 m, and the depth of borehole DP-7 reached about 16 m. In addition to the core samples, we gathered organic samples for the C-14 dating in order to build up the time references of the possible fault or mass movement activities. A borehole SAA (Shape Accel Array) Inclinometer was installed in DP-6 for monitoring the long-term creeping of the Lichi mélange on the hillslope. The instrument configurations in our study are designed to probe into the spatial structures

of the frontal deformation zone in as detailed a manner as possible under the constraint of staying within an affordable budget.

4. Data-processing approaches

We have processed the ERI measurements with 2D inversion code, EarthImager2D™ (AGI, 2009). The software employs (1) iterative algorithms with Dirichlet or mixed boundary conditions (Dey and Morrison, 1979) for forward simulation and (2) conjugated-gradient inversion schemes for estimating the subsurface resistivity structures. In the inversion scheme, we chose to minimize the L1 norm because the blocky model inverted with the L1 norm is more suitable for fracture or fault detection than the smooth model with the L2 norm (Loke et al., 2003).

We collected the resistivity measurements with every possible combination of the electrode configurations in the field. A total of 66,858 and 70,345 measurements were collected in the ERI-I and ERI-II survey lines, respectively. However, both the excessive number of measurements and the noise in some of the data hampered our effort to compute the inversion with all measurements. It is recommended that researchers use the Wenner and Schlumberger arrays to select data that have high signal-to-noise ratios (e.g., Nguyen et al., 2007). By selecting the measurements from only the Wenner- and Schlumberger-type arrays, we ended up with data that had repeated errors of less than 3% and reciprocal errors of less than 5% (Chang et al., 2011; Dahlin, 1996; Dahlin and Zhou, 2004; Uhlemann et al., 2017). We are able to use 11,101 measurements for ERI-I and 12,178 measurements for ERI-II for the resistivity inversion.

5. Results

5.1. The borehole cores

Fig. 3 presents the lithology of the cores from the four boreholes (DP-4, DP-1, DP-6, and DP-7). From the core samples, we identified three major geological components at a depth of within 30 m at the Dapo site: the Lichi mélange, the colluvial gravels with mixed sedimentary and volcanic clasts, and the alluvial gravels with mainly metamorphic clasts. On the hanging wall of the Chihshang Fault is the Lichi mélange, whose clay matrix contains sporadic exotic rocks. The Lichi mélange was found at a depth of between 0 and 13 m in the DP-6 borehole and 0 and 11 m in the DP-7 borehole. The clayey Lichi mélange lies above the colluvial gravels in these two boreholes. The colluvial gravels consist of brownish, poorly sorted, matrix-supported clasts originating from volcanic and sedimentary rocks in the Costal Ranges. And in borehole DP-6, we found that the sediments with metasandstone pebbles from the Central Ranges lie under the colluvial gravel layers at a depth

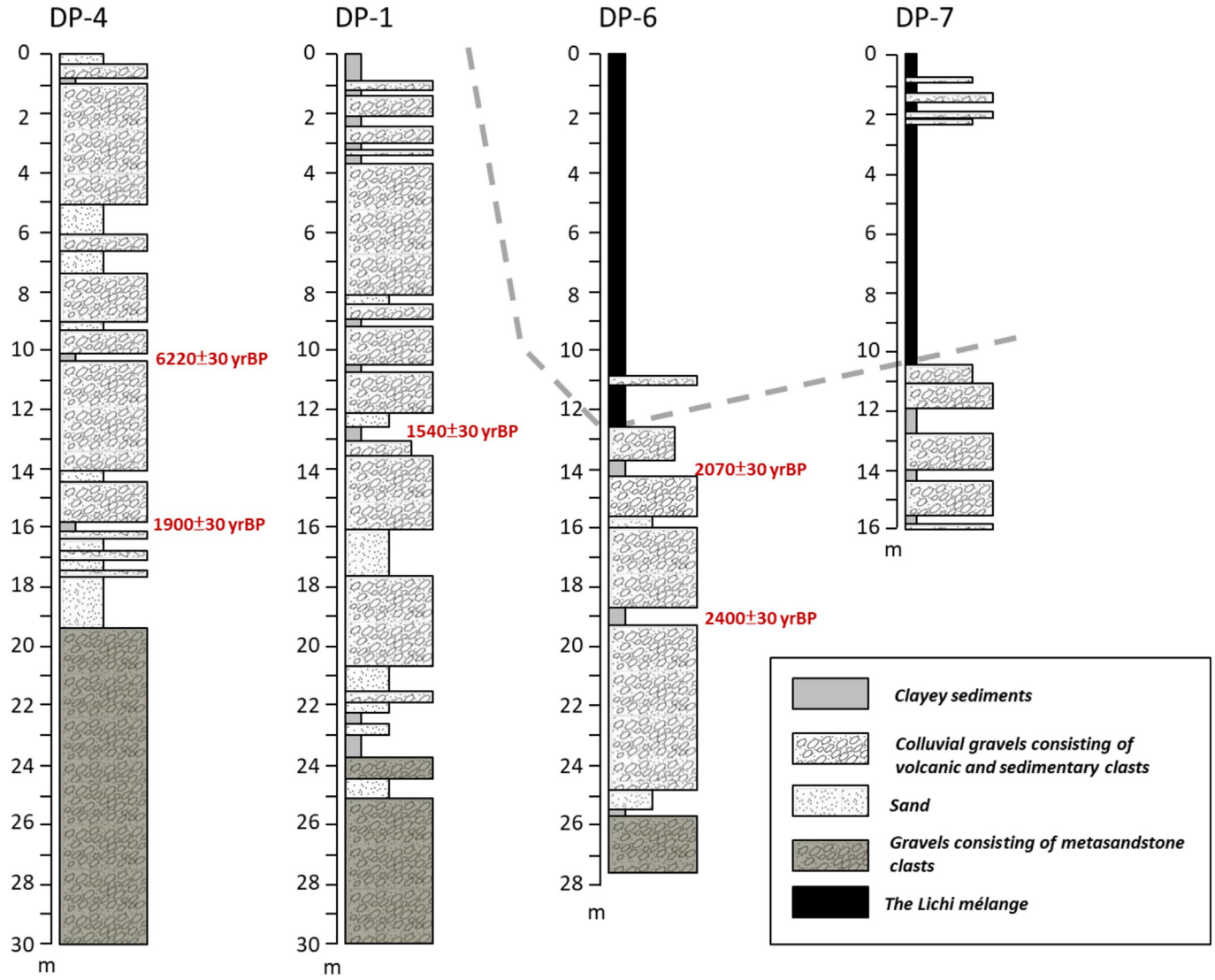

Fig. 3. Geological columns of the boreholes DP-4, DP-1, DP-6, and DP-7. The dashed grey line shows the contact between the Lichi mélange on the hanging wall and the gravel deposits on the footwall.

Table 1
The C-14 dating results.

Sample no.	DPE6_1955	DPE6_1475	DPE4_1585	DPE4_1035	DPE1_1270
Location	DP-6	DP-6	DP-4	DP-4	DP-1
Depth (m)	14.75	19.55	15.85	10.35	12.7
Material	Organic sediment	Organic sediment	Organic sediment	Organic sediment	Organic sediment
$^{13}C(^{0}/_{00})$	−15.0	−14.9	−13.1	−19.8	−13.3
^{14}C(pMC)	74.2 ± 0.3	77.3 ± 0.3	78.9 ± 0.3	46.1 ± 0.2	82.6 ± 0.3
Conventional age (BP)	2400 ± 30	2070 ± 30	1900 ± 30	6220 ± 30	1540 ± 30

of 26–28 m. The same fluvial gravels with metasandstone pebbles also appear in DP-1 and DP-4 at a depth of 24–30 m and 19–30 m respectively. Since the surface elevations for DP-6, DP-1, and DP-4 are about 283.5 m, 280 m, and 278 m above the mean sea level, the top of the fluvial gravel layer is at about the same elevation in the boreholes DP-6, DP-1, and DP-4.

Owing to the plastic properties of clays, we discovered no sharp contacts or distinctive fault zones between the Lichi mélange and the gravel layers in either DP-6 or DP-7. The two boreholes DP-6 and DP-7 were about 3 m apart with about 1-m in height difference. When we used the contacts between the Lichi mélange and the gravels to estimate the dipping angle of the Chihshang Fault, we came up with a northwesterly angle of about 45°, which contrasts with researchers' previous outcrop observations of the dipping of the Chihshang fault plane.

5.2. The C-14 dating

In addition, we did not find the Lichi mélange in boreholes DP-1 and DP-4. The findings suggest that the two boreholes are located in the footwall of the Chihshang Fault. The unconsolidated sediments in DP-1 and DP-4 are composed of brownish, poorly sorted, matrix-supported colluvial sediments, which themselves are composed of andesitic gravels and are on top of the fluvial gravels which clasts are mainly metasandstone. The contacts between the colluvial sediments and the fluvial gravels are at depths of about 24 and 19 m in the DP-1 and DP-4 boreholes, respectively.

To verify the possible age of the slumping and the fault movements, we took 5 organic samples from the cores in the layer of colluvial gravels and subjected the samples to C-14 dating, conducted by the Beta Lab. The results, shown in Table 1, reveal that the organic sediments in the colluvial gravels dates back to a period between 1500 and 2000 years Before the Present (yrBP). The one exception is the DP-4 organic sample: its dated age is about 6220 yrBP at a depth of 10 m, but about 1900 yrBP at a depth of 16 m. The abnormal age of the DP-4 sample suggests that it may be the reworked sediments because the measured age is illogical in comparison with the measured ages of the other samples. Moreover, the dated samples are all from the organic deposits in the colluvial gravel layers, and their ages seem to increase laterally beginning in the region near the actual fault plane. These facts suggest that the colluvial sediments are accreted not only vertically but also laterally from their origin on the hanging wall of the Chihshang Fault.

5.3. The resistivity results

Fig. 4a and b show the inverted two-dimensional model of the ERI survey lines, ERI-I, and ERI-II, respectively. The inversion reached optimal solutions after 7 iterations and 6 iterations for ERI-I and ERI-II, respectively. And the RMS error of inversions for ERI-I and ERI-II are 7.04% and 7.90%, respectively.

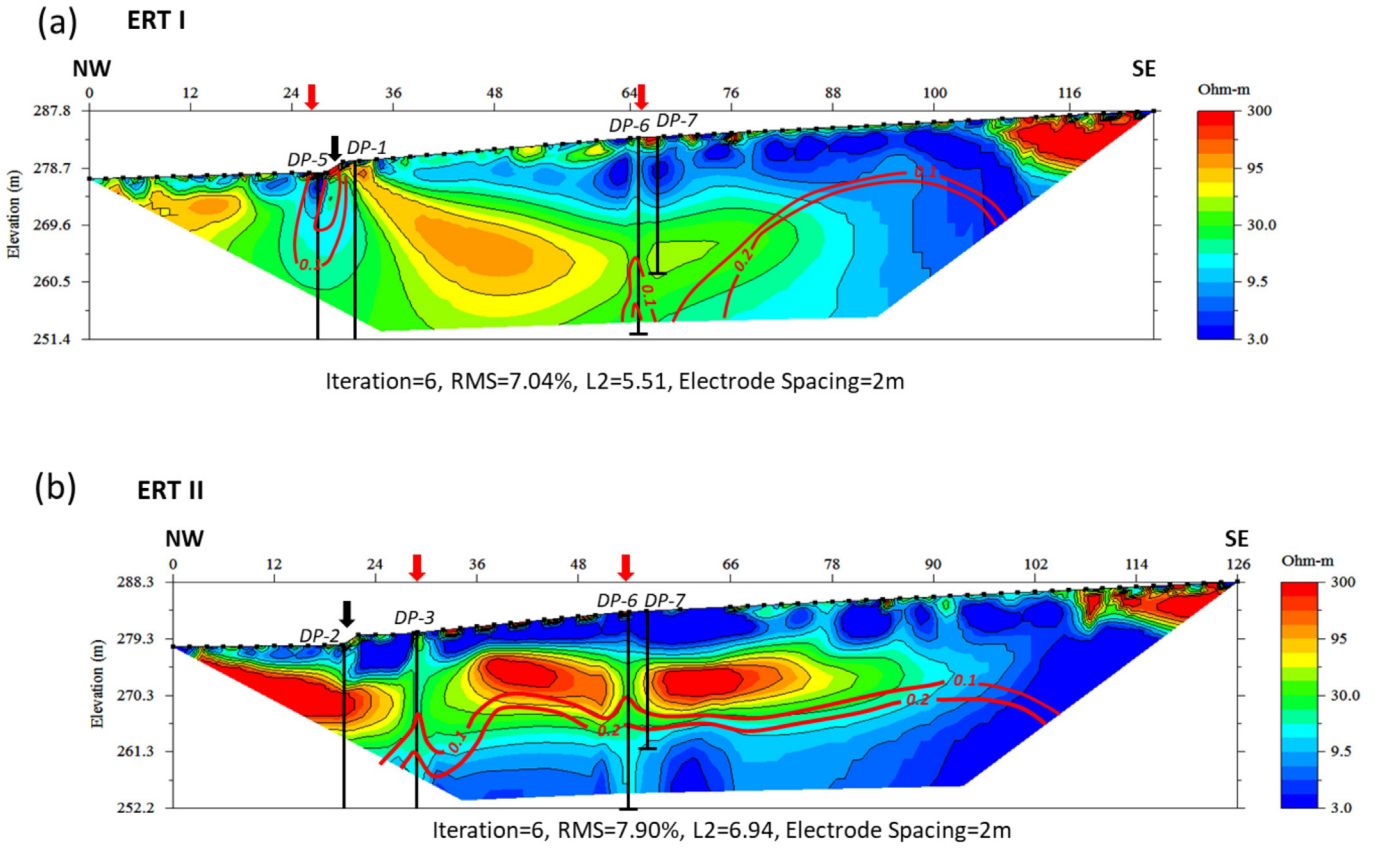

Fig. 4. The inverted resistivity model of (a): ERI-I and (b): ERI-II. The nearby boreholes are projected on the profile shown as the black vertical lines. The black arrow shows the position of the topographic scarp. The red arrow denotes the vertical resistivity artifact structures caused by the boreholes. The red contours are the DOI index suggested by Oldenburg and Li (1999) for the evaluation of the depth of investigations.

In both figures, we also show the contours of empirical depth of Investigation (DOI) index that is proposed by Oldenburg and Li (1999) and modified by Deceuster et al. (2014) for the appraisal of the DOI. Oldenburg and Li (1999) suggested that the interpretations for where the DOI index higher than 0.1 and 0.2 should be avoided. In the study we used the DOI index value of 0.2 as the cut-off value. Noted that the region deeper than 265-m in elevation in ERI-II is located at the region with DOI index larger than 0.2. The resistivity structures below 265-m in ERI-II may be poorly resolved, and one should be careful for making any interpretations from the resistivity structures deeper than 265-m with the inverted image of ERI-II.

The resistivities of the unconsolidated sediments and the Lichi mélange range from 1 Ω-m to slightly over 1000 Ω-m in the two profiles. We observed the vertical low-resistivity structures that truncate the horizontal resistivity structures at depths of about 24–30 m and 64–68 m at the horizontal distance mark in ERI-I, and about 28–32 m and 52–56 m at the horizontal distance mark in ERI-II. Because these structures are associated with the locations of borehole electrode arrays and the retaining wall, we have concluded that they are artifacts from man-made structures.

As Fig. 5 shows, we compared the core logs and the 1:1 resistivity profiles of ERI-I with those of ERI-II because most materials exhibit resistivities between 3 and 300 Ω-m. The matrix of the Lichi mélange consists mainly of clays and, thus, shows a low resistivity response of less than 10 Ω-m in both of the ERI image sets. By contrast, the colluvial gravels and sands are more resistive than the Lichi mélange, since they have fewer clay contents than the Lichi mélange. The colluvial gravels underlying the Lichi mélange have resistivities that are higher than 20 Ω-m in general. Therefore, we can distinguish the Lichi mélange from the underlying colluvial gravel layers in the resistivity profiles. On the other hand, the fluvial gravel layer with metasandstone pebbles seem to exhibit a low resistivity response in ERI-I, with the resistivity less than 30 Ω-m under the colluvial gravels.

As shown in Fig. 5a, we found that the contact between the conductive Lichi mélange and the relatively resistive colluvial gravels correlates well to the corresponding contact in the core logs of DP-6 in ERI-I. The contact between the Lichi mélange and the underlying colluvial gravels is characterized by a wavy surface and is deepest near DP-6. The depth of the contact between the colluvial gravels and the underlying fluvial gravels in core logs correlates to the resistivity interface, where the resistivity declining from over 30 Ω-m to less than 20 Ω-m. The thickness of the colluvial gravel layer seems to decrease in a southeastward direction, and the layer itself is eventually pinched out at the region between 88 and 105 m relative to the horizontal distance mark in ERI-I. By contrast, the depths of the contacts between the Lichi mélange and the colluvial gravel layer show an offset that is about 3–5 m shallower than the contact depths registered in the core logs of DP-6. Aside from the mismatch of the contact depths, the resistive colluvial gravel layer shows a good horizontal extension *in ERI-II* and pinches out at about 90 m at the distance mark (see Fig. 5b).

6. Discussion

Because the resistive colluvial gravel layer exhibits good lateral extension in both the resistivity images and the core logs, and because we observed no obvious disturbance at the contacts between the colluvial and fluvial gravel layers in most of the ERI-I and ERI-II profiles, we conclude that the creeping Chihshang fault may be located in the

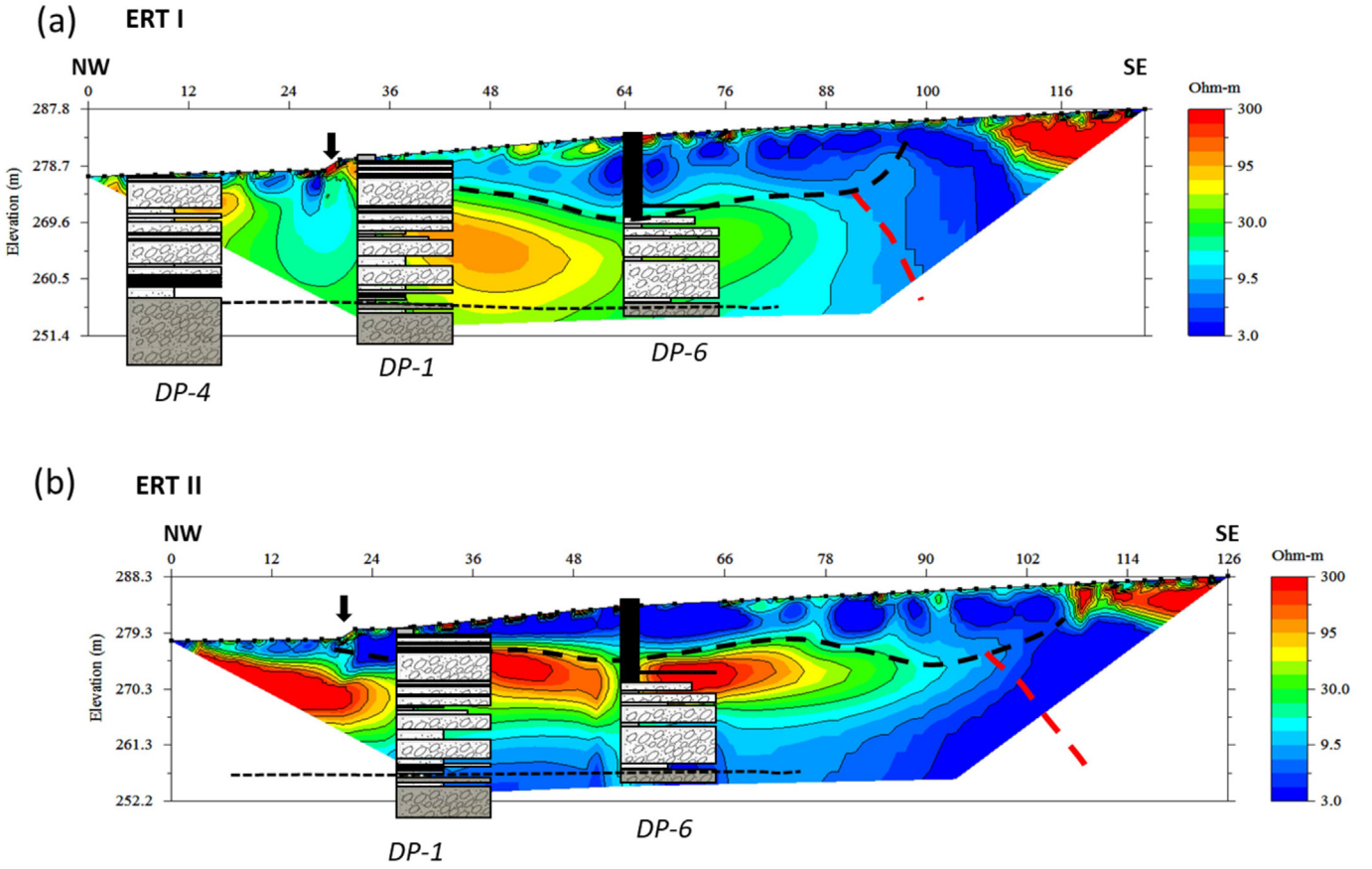

Fig. 5. (a): The 1:1 resistivity profile and the explanation of the results from ERI-I. (b): The 1:1 resistivity profile and the explanation of the results from ERI-II. The thick black dashed line shows the contact between the slumping Lichi mélange and the underlying colluvial gravels, the thin black dashed line represents the contact between the colluvial and the fluvial gravels, and the red dashed line suggests the possible fault trace of the Chihshang Fault.

southeastern corner of the resistivity profiles, where the gravels pinched out, or be truncated by the fault plane. Hence the fault is likely located at the place that the colluvial gravels are pinched out as indicated in Fig. 5. Furthermore, the resistivity images of both ERI-I and ERI-II show that the contact between the Lichi mélange and the colluvial gravels corresponds to a wavy, curved surface. The contact surface between the conductive Lichi mélange and the resistive gravels dip toward the northwest at an angle of about 45–55° near the top of the slope. Yet the dipping of the contact seems to turn into a low angle of 30–35° to the southeast, near the surface scarp, in both the ERI-I and ERI-II profiles. In ERI-I, we found that the depths of the curvature contact surface between the Lichi mélange and the gravels can reach a maximum depth of about 10–13 m in the center of the profile. The curvature contact's outcrop on the downhill side is at the toe of the hill, where the fault scarp of the Chihshang Fault was thought to be and where the creepmeters were installed. According to the facts above the topographic scarp that was thought to be the fault scarp is perhaps not the outcrop of the Chihshang fault's actual fault trace, and likewise, the Lichi mélange above this surface actually may consist of the slumping materials. The slumping movement of the materials from the hanging wall causes the curvature rupture surface between the Lichi formation and its underlying gravels. The actual fault plane of the Chihshang fault is located under the slumping Lichi mélange in the southeastern part of the resistivity profiles ERI-I and ERI-II, instead of in the hillslope's toe position.

As in Mu et al. (2011), one may argue that the west-dipping contact between the Lichi mélange and the gravels near the top of the slope is the back thrust structure of the Chihshang Fault. If the contact is the back-thrust structure, we should be able to observe the relative westward movements within the tongue-like mass of the Lichi mélange. To verify our slumping assumptions from the resistivity images and borehole cores, we installed an SAA tiltmeter in DP-7 at a depth ranging from 5 m to 15 m. The SAA sensors were placed at a vertical spacing of 0.5 m. From January 1 to March 22 of 2017, we recorded the horizontal displacement with SAA and identified several shear zones in DP-7 (Fig. 6). For only 81 days of observation, the accumulated displacement regarding the SAA tiltmeter's position at a depth of 15 m extended over 5.3 mm westward, which is similar to the shortening rate measured from the regional GPS measurements and creepmeters (about 2–3 cm/yr). In addition, we identify several distinctive shear zones in the Lichi mélange with a displacement of over 0.3 mm at the depths of 6.5 m, 8 m, 10 m, 11 m and 12 m from the relative displacement between the two vertical adjacent sensors.

With the high-resolution resistivity images, we have been able to resolve the spatial relationships of the rocks and sediments, and to discriminate amongst the slumping ruptures from the fault planes. We found that the tongue-like body of Lichi mélange may be the result mainly of slumping induced by the inter-seismic creeping and mass movements, and the fault trace of the Chihshang Fault is not located at the toe of the hillslope at the Dapo site. The resistivity profiles suggest that the actual fault plane is in the uphill portion of the two survey lines' southeastern region. The borehole records and tiltmeter's data also agree with the findings from the resistivity images. From the principle of superposition, we conclude that the initiation of current slumping that caused the tongue-like body of Lichi mélange took place at least sometime after about 2000 yrBP. In addition, the resistivity images suggest that the fault plane is located on the upper rupture surface of the slumping body. The later mass-movement, due to gravity, erosion and inter-seismic fault creeping, may have helped re-modify the landscape and moved the frontal scarp of the hanging-wall materials farther away from the actual fault trace since 2000 yrBP as shown in Fig. 7. From the evidences, we concluded that the fluvial gravels originating from the Central Range were deposited on the Lichi mélange before 3000 years (Fig. 7a). The Costal Range's colluvial deposits were then

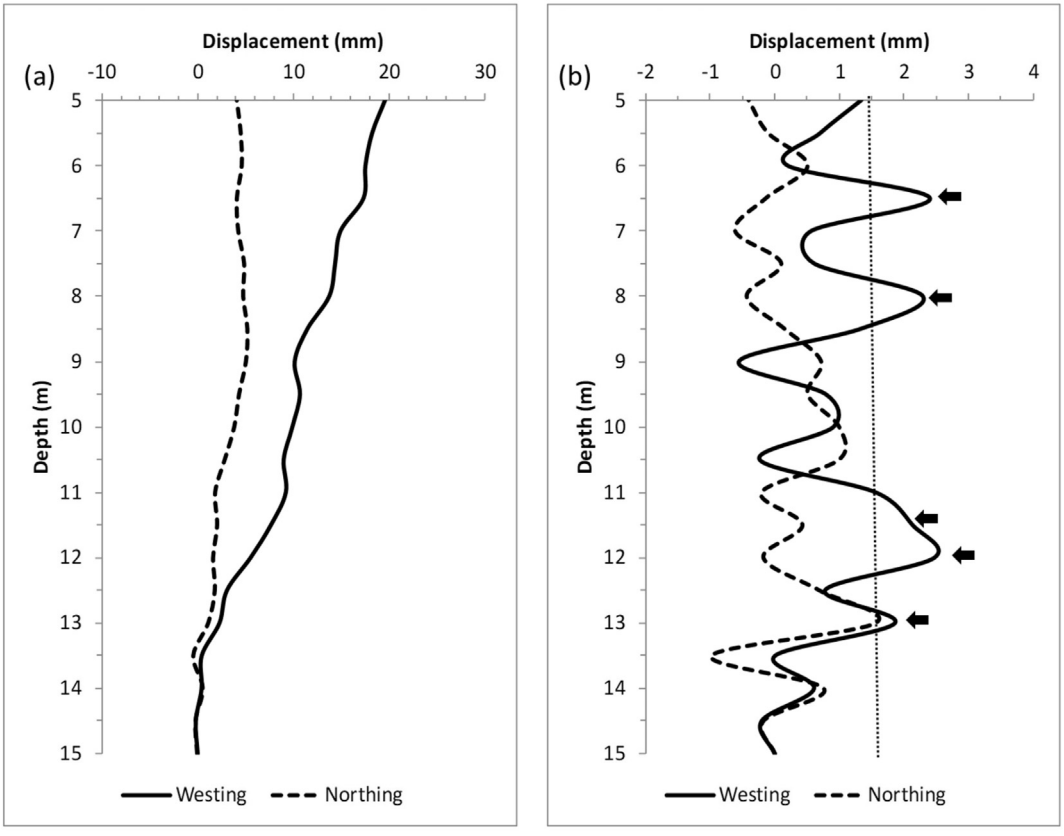

Fig. 6. (a): The accumulated westing and northing displacements recorded in the SAA Inclinometer. (b): The relative displacements calculated with the data from the SAA Inclinometer. The arrows show the locations that have larger westing displacements.

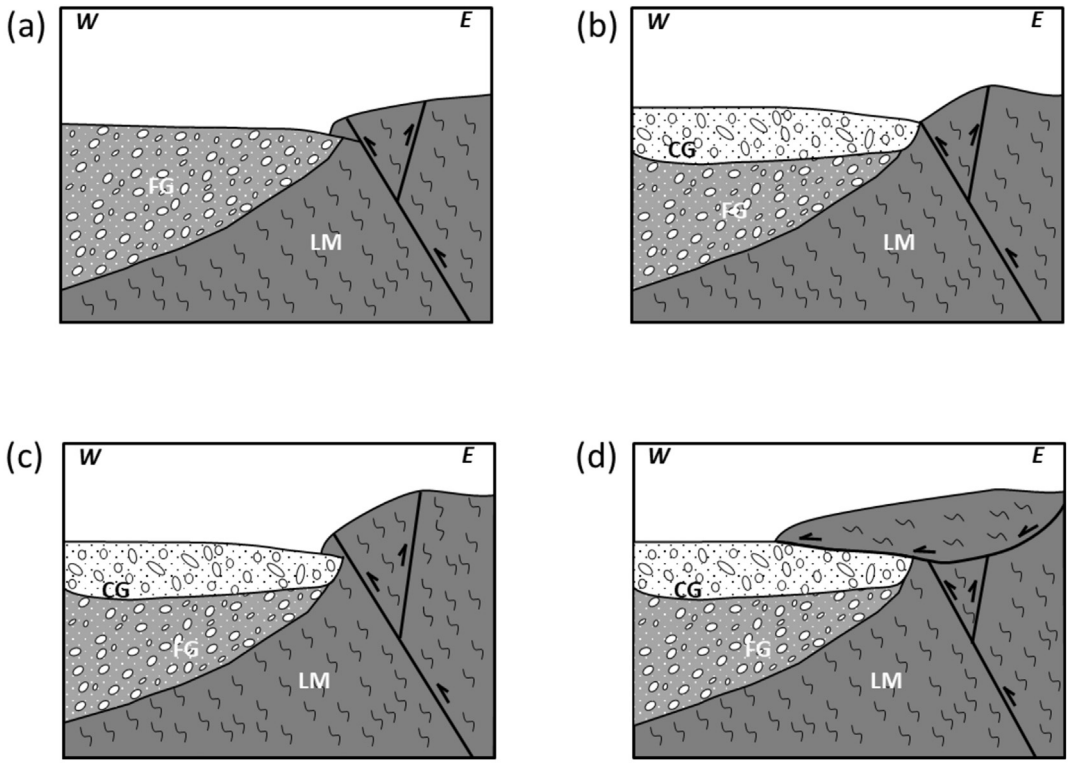

Fig. 7. The schematic diagrams showing the evolution of the frontal deformation zone at the Dapo site. (a): The deposition of the fluvial gravels (FG) originating from the Central Range on the heavily-sheared Lichi mélange (LM) in at least 3000 years ago. (b): The start of the accumulation of the Costal Range's colluvial deposits (CG) between 2000 and 3000 years ago. (c): The coseismic movements of the Chihshang Fault, which resulted in the uplifted Lichi mélange and narrow frontal deformation zone after the deposition of the colluvial gravels. (d): The recent slumping mass movements causing modifications to the frontal deformation zone after 2000 years ago.

accumulated and stopped laterally by the uplifted hill of Lichi mélange about 2000 to 3000 years ago (Fig. 7b). The coseismic movements of the Chihshang Fault, which resulted in the uplifted Lichi mélange and narrow frontal deformation zone (Fig. 7c). Lastly, the slumping mass movements took place after 2000 years ago modified the frontal deformation zone (Fig. 7d).

The coseismic faulting may have caused the uplifted hanging wall and narrow deformation zone, yet the later slumping modification of the landscape moved the topographic scarp farther away from the actual fault trace in the inter-seismic period. As a result, researchers using near-surface geophysical methods would do well to further probe the frontal deformation zones and their spatial relationships to the actual fault trace of the active faults if such relationships may reveal the recurrence rate of the faults.

7. Conclusions

We have conducted surface electrical resistivity surveys and have examined four borehole cores in order to understand the near-surface structures within the frontal deformation zone of the Chihshang Fault at the Dapo site in eastern Taiwan's Taitung County. Previous studies suggested that the fault plane of the Chihshang Fault is outcropped at the toe of the hillslope at the Dapo elementary school. However, we discovered that a tongue-like body of the Lichi mélange was laid over the colluvial gravel layers with a curvature contact surface in Dapo from the high resolution resistivity images and the borehole logs. We concluded that the tongue-like body is the slumping mass originated mainly from the Lichi mélange on the hanging wall. And the toe of the slumping mass is at the position where the fault trace of the Chihshang Fault was thought to be. The actual fault plane of the Chihshang fault is located under the slumping Lichi mélange in the southeastern part of the resistivity profiles ERI-I and ERI-II, instead of in the hillslope's toe position.

The C-14 dating shows that the slumping may have taken place within the last 2000 years. The topographic modification by the inter-seismic mass movement makes it difficult for researchers to identify the actual fault traces in the regions suffered by heavy weathering and transportation effects. Without a non-invasive geophysical investigation into the near-surface spatial relationships of the fault zone structures, one may make a wrong geological conclusion from limited boreholes and trenching observations, if they took place in the wrong positions. In addition, we concluded that coseismic faulting may have caused the uplifted hanging wall and narrow deformation zone, yet the later slumping modification of the landscape induced by fault creeping moved the topographic scarp farther away from the actual fault trace in the inter-seismic period.

From the C-14 dating results, we conclude that the initiation of current slumping took place at least sometime after about 2000 yrBP at the Dapo site. The distance between the topographic scarp and the actual fault trace is about 70 m. Therefore, the displacement velocity of the front of the slumping mass is about 3.5 cm/yr, which is slightly higher than that estimated from the creepmeter (2–3 cm/yr). The observations in our study suggest that the spatial relationships between the locations of modified topographic scarp and the actual fault trace may reveal the recurrence rate of the creeping Chihshang faults. The spatial relationships may be used as a proxy to evaluate the recurrence rate of the creeping faults, if there are no additional dating records available. In order to verify our current assumptions, future research using high-resolution near-surface geophysical methods should consider reviewing the frontal deformation zones of the active faults in detail.

Acknowledgements

This study has been supported by the Central Geological Survey of the Ministry of Economic Affairs, R.O.C. under project # 106-5226904000-02-01.

References

AGI, 2009. Instruction Manual for EarthImager 2D Version 2.4.0. Advanced Geosciences, Inc., Austin, Texas.

Angelier, J., Chu, H.-T., Lee, J.-C., 1997. Shear concentration in a collision zone: kinematics of the Chihshang Fault as revealed by outcrop-scale quantification of active faulting, Longitudinal Valley, eastern Taiwan. Tectonophysics 274 (1), 117–143.

Angelier, J., Chu, H.-T., Lee, J.-C., Hu, J.-C., 2000. Active faulting and earthquake hazard: the case study of the Chihshang fault, Taiwan. J. Geodyn. 29 (3), 151–185.

Cai, J., McMechan, G.A., Fisher, M.A., 1996. Application of ground-penetrating radar to investigation of near-surface fault properties in the San Francisco Bay region. Bull. Seismol. Soc. Am. 86 (5), 1459–1470.

Carpenter, B., Marone, C., Saffer, D., 2011. Weakness of the San Andreas Fault revealed by samples from the active fault zone. Nat. Geosci. 4 (4), 251–254.

Chang, P.-Y., Chang, S.-K., Liu, H.-C., Wang, S.C., 2011. Using integrated 2D and 3D resistivity imaging methods for illustrating the mud-fluid conduits of the Wushanting Mud Volcanoes in Southwestern Taiwan. Terr. Atmos. Ocean. Sci. 22 (1), 1–14.

Chen, W.-S., Lee, K.-J., Lee, L.-S., Streig, A.R., Rubin, C.M., Chen, Y.-G., Yang, H.-C., Chang, H.-C., Lin, C.-W., 2007. Paleoseismic evidence for coseismic growth-fold in the 1999 Chichi earthquake and earlier earthquakes, central Taiwan. J. Asian Earth Sci. 31 (3), 204–213.

Chow, J., Angelier, J., Hua, J.-J., Lee, J.-C., Sun, R., 2001. Paleoseismic event and active faulting: from ground penetrating radar and high-resolution seismic reflection profiles across the Chihshang Fault, eastern Taiwan. Tectonophysics 333 (1), 241–259.

Chuang, R.Y., Johnson, K.M., Kuo, Y.T., Wu, Y.M., Chang, C.H., Kuo, L.C., 2014. Active back thrust in the eastern Taiwan suture revealed by the 2013 Rueisuei earthquake: evidence for a doubly vergent orogenic wedge? Geophys. Res. Lett. 41 (10), 3464–3470.

Colella, A., Lapenna, V., Rizzo, E., 2004. High-resolution imaging of the High Agri Valley Basin (Southern Italy) with electrical resistivity tomography. Tectonophysics 386 (1), 29–40.

Dahlin, T., 1996. 2D resistivity surveying for environmental and engineering application. First Break 14, 275–283.

Dahlin, T., Zhou, B., 2004. A numerical comparison of 2D resistivity imaging with 10 electrode arrays. Geophys. Prospect. 52, 379–398.

Deceuster, J., Etienne, A., Tanguy, R., Nguyen, F., Kaufmann, O., 2014. A modified DOI based method to statistically estimate the depth of investigation of dc resistivity surveys. J. Appl. Geophys. 103, 172–185.

Dey, A., Morrison, H.F., 1979. Resistivity modeling for arbitrarily shaped three-dimensional structures. Geophysics 44 (4), 753–780.

Harris, R.A., 2017. Large earthquakes and creeping faults. Rev. Geophys. 55 (1):169–198. https://doi.org/10.1002/2016RG000539.

Hsu, T., 1962. Recent faulting in the Longitudinal Valley of eastern Taiwan. Mem. Geol. Soc. China 1.

Lin, A., Wang, S., Hung, J., Wu, M., Liu, C., 2007. Lithostratigraphy of the Taiwan Chelungpu-fault Drilling Project-a borehole and its neighboring region, central Taiwan. Terr. Atmos. Ocean. Sci. 18 (2), 223.

Lee, J.-C., Angelier, J., Chu, H.-T., Hu, J.-C., Jeng, F.-S., 2001. Continuous monitoring of an active fault in a plate suture zone: a creepmeter study of the Chihshang Fault, eastern Taiwan. Tectonophysics 333 (1), 219–240.

Lee, J.C., Angelier, J., Chu, H.T., Hu, J.C., Jeng, F.S., Rau, R.J., 2003. Active fault creep variations at Chihshang, Taiwan, revealed by creep meter monitoring, 1998–2001. J. Geophys. Res. Solid Earth 108 (B11).

Lee, J.-C., Rubin, C., Mueller, K., Chen, Y.-G., Chan, Y.-C., Sieh, K., Chu, H.-T., Chen, W.-S., 2004. Quantitative analysis of movement along an earthquake thrust scarp: a case study of a vertical exposure of the 1999 surface rupture of the Chelungpu fault at Wufeng, Western Taiwan. J. Asian Earth Sci. 23 (2), 263–273.

Loke, M.H., Acworth, I., Dahlin, T., 2003. A comparison of smooth and blocky inversion methods in 2D electrical imaging surveys. Explor. Geophys. 34 (3), 182–187.

McClymont, A.F., Green, A.G., Villamor, P., Horstmeyer, H., Grass, C., Nobes, D.C., 2008. Characterization of the shallow structures of active fault zones using 3-D ground-penetrating radar data. J. Geophys. Res. Solid Earth 113 (B10).

Mu, C.-H., Angelier, J., Lee, J.-C., Chu, H.-T., Dong, J.-J., 2011. Structure and Holocene evolution of an active creeping thrust fault: the Chihshang fault at Chinyuan (Taiwan). J. Struct. Geol. 33 (4), 743–755.

Nguyen, F., Garambois, S., Chardon, D., Hermitte, D., Bellier, O., Jongmans, D., 2007. Subsurface electrical imaging of anisotropic formations affected by a slow active reverse fault, Provence, France. J. Appl. Geophys. 62 (4), 338–353.

Oldenburg, D.W., Li, Y., 1999. Estimating depth of investigation in DC resistivity and IP surveys. Geophysics 64 (2), 403–416.

Shea, K.S., et al., 2014. Research on Structural Characteristics of Important Active Faults (1/4) Rep. Central Geological Survey, Ministry of Economics, Taipei (14 pp.).

Suski, B., Brocard, G., Authemayou, C., Muralles, B.C., Teyssier, C., Holliger, K., 2010. Localization and characterization of an active fault in an urbanized area in central Guatemala by means of geoelectrical imaging. Tectonophysics 480 (1), 88–98.

Suzuki, K., Toda, S., Kusunoki, K., Fujimitsu, Y., Mogi, T., Jomori, A., 2000. Case studies of electrical and electromagnetic methods applied to mapping active faults beneath the thick quaternary. Eng. Geol. 56 (1–2):29–45. https://doi.org/10.1016/S0013-7952(99)00132-5.

Tsai, Y.B., Teng, T.L., Chiu, J.M., Liu, H.L., 1977. Tectonic implications of the seismicity in the Taiwan region. Mem. Geol. Soc. China 2, 13–42.

Uhlemann, S., Kuras, O., Richards, L.A., Naden, E., Polya, D.A., 2017. Electrical resistivity tomography determines the spatial distribution of clay layer thickness and aquifer vulnerability, Kandal Province, Cambodia. J. Asian Earth Sci. 147:402–414. https://doi.org/10.1016/j.jseaes.2017.07.043.